Electronic Supplementary Material (ESI) for Soft Matter

Supporting Information

Synthesis and redox-responsive self-assembly of ferrocene grafted Anderson-type polyoxometalate complexes

Yi Yan, Bao Li, Qingyi He, Zhenfeng He, Hui Ai, Huanbing Wang, Zhendong Yin, and Lixin Wu*

State Key Laboratory of Supramolecular Structure and Materials, College of Chemistry, Jilin University, Changchun, P. R. China,

E-mail: wulx@jlu.edu.cn; Fax: +86 431 85193421; Tel: +86 431 85168481

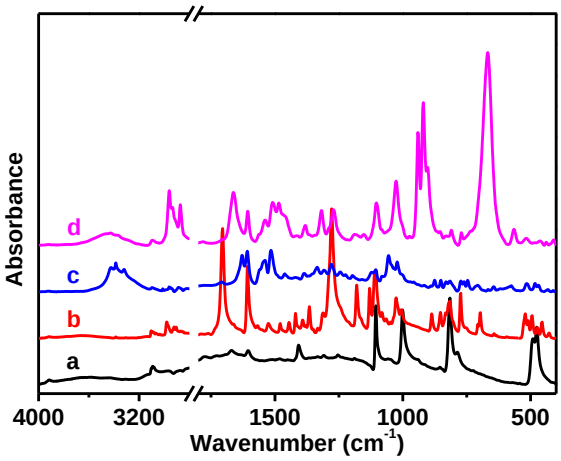

Figure S1. FT-IR spectra of a) ferrocene, b) ethyl 4-ferrocenylbenzoate (2), c) N-tris(hydroxymethyl)methy (4-ferrocenyl)benzamide (3), and d) SEOP–1.

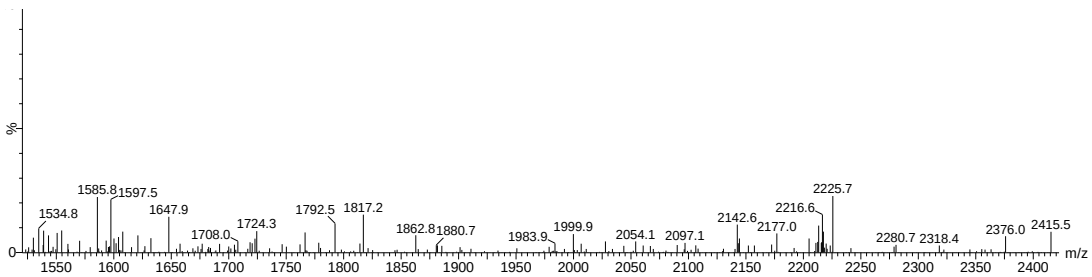

Figure S2. ESI-MS of SEOP–1.

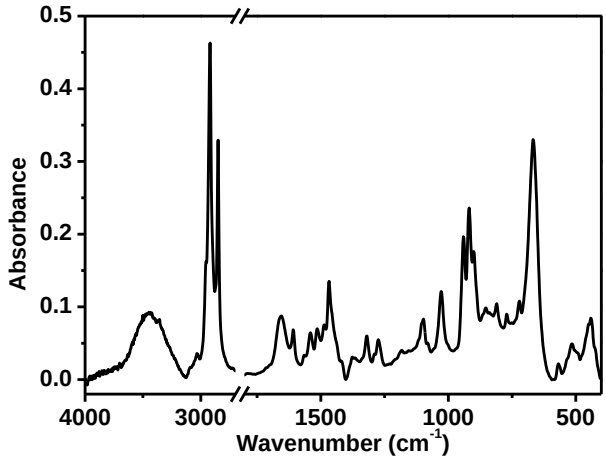

Figure S3. FT-IR spectrum of SEOP–2.

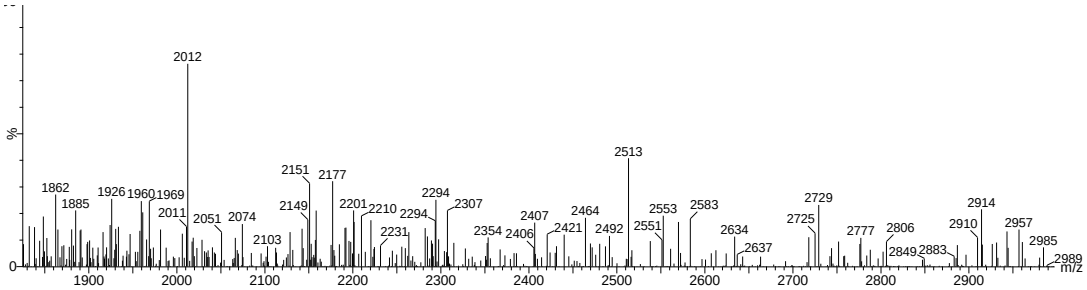

Figure S4. ESI-MS of SEOP–2.

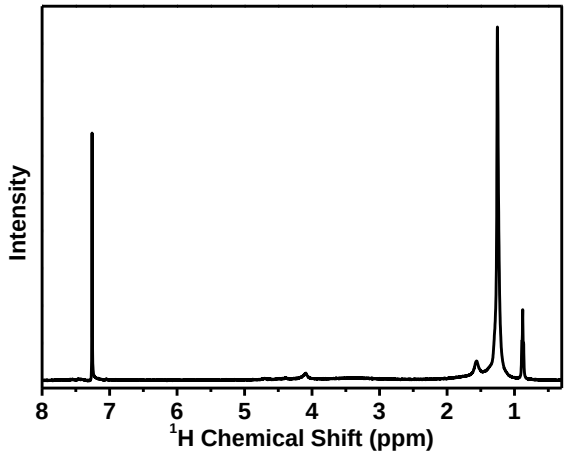

Figure S5. ^{1}H NMR spectrum of SEOP–2.

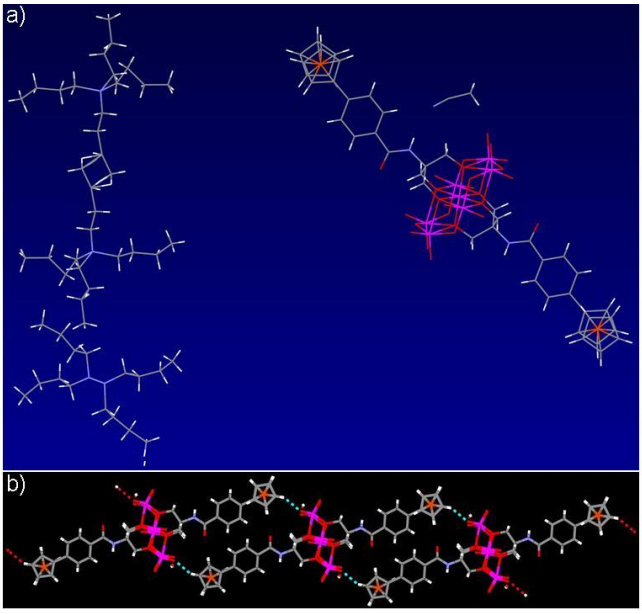

Figure S6. (a) Single crystal structure of SEOP–1, there are three TBA surfactant molecules and one POM in one SEOP–1; (b) extended crystal structure connected by hydrogen bond between terminal oxygen of $MnMo_6$ cluster and hydrogen of ferrocene group in SEOP–1.

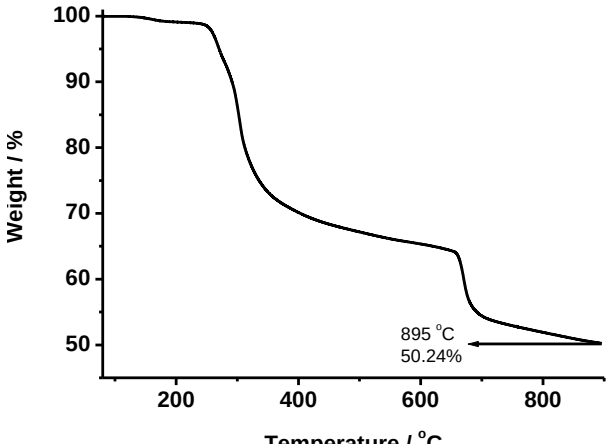

Figure S7. TGA diagram of SEOP–1.

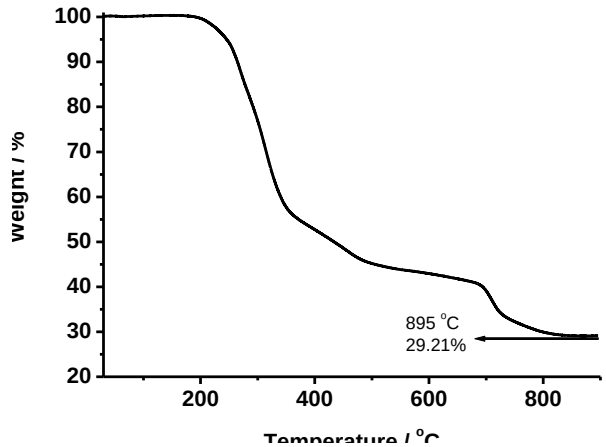

Figure S8. TGA diagram of SEOP–2.

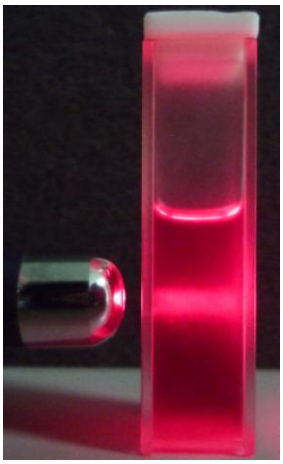

Figure S9. Image of the Tyndall scattering of SEOP–2 in $CHCl_3$ and methanol 4:1 (v/v) mixture solvent.

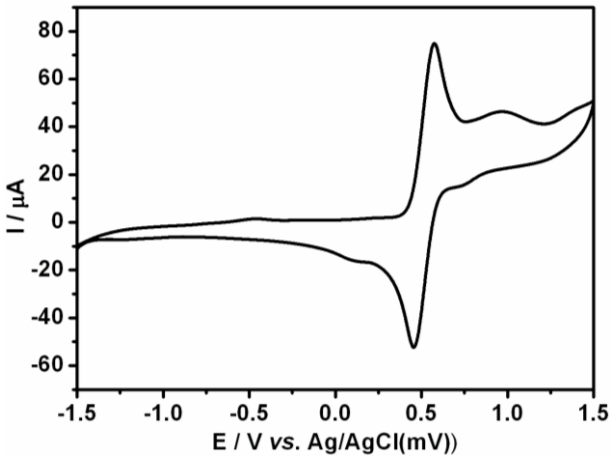

Figure S10. Cyclic voltammogram of virgin ferrocene in DMF at a scan rate of 100 mV/s.

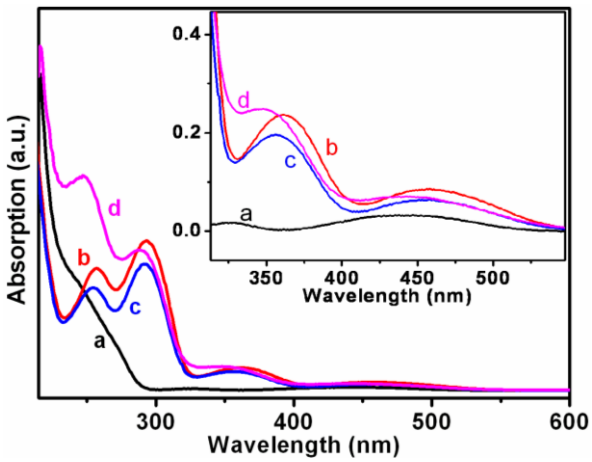

Figure S11. UV-Vis spectra of (a) ferrocene, (b) ethyl 4-ferrocenylbenzoate (2), (c) N-tris(hydroxymethyl)methy (4-ferrocenyl)benzamide (3), and (d) SEOP–1 in the corresponding solution, where the inset is an enlarge section from the range of 315-525 nm.

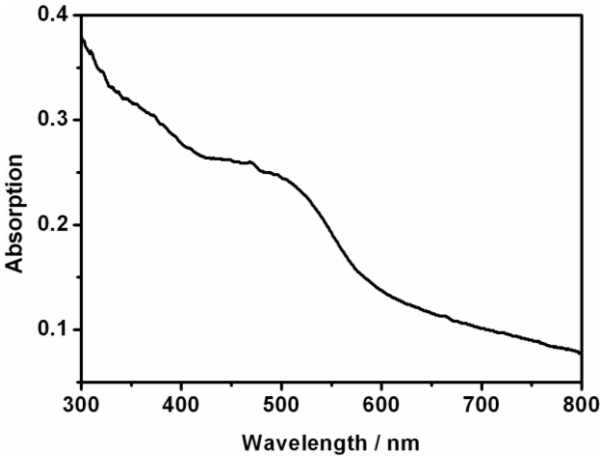

Figure S12. Solid diffusive reflective UV-Vis spectrum of SEOP–1.

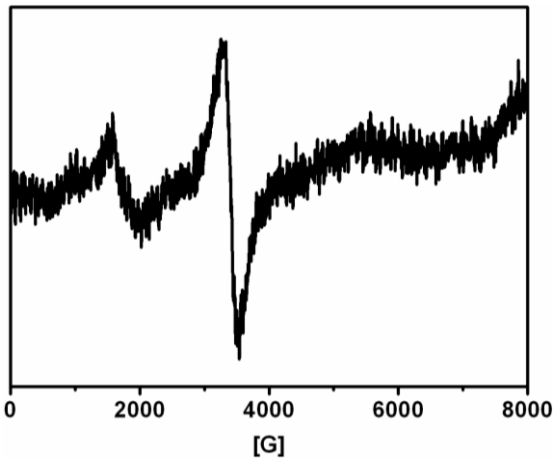

Figure S13. EPR spectrum of SEOP–1 powder measured at room temperature.

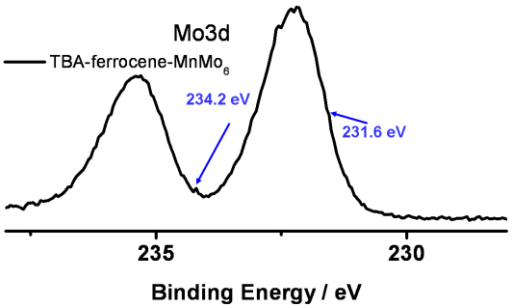

Figure S14. Mo3d XPS result of SEOP–1.

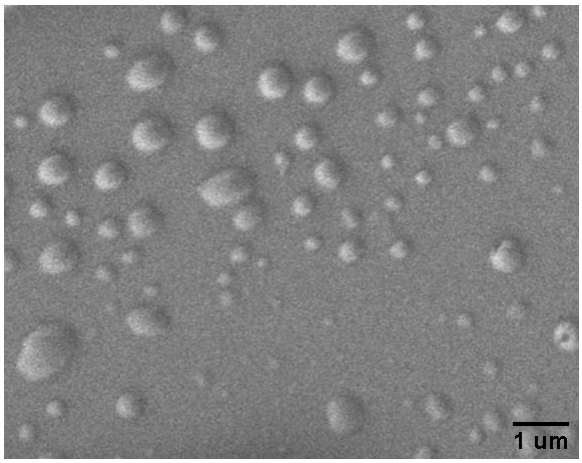

Figure S15. SEM image of SEOP–1 self-assemblies in CH_3CN solution.

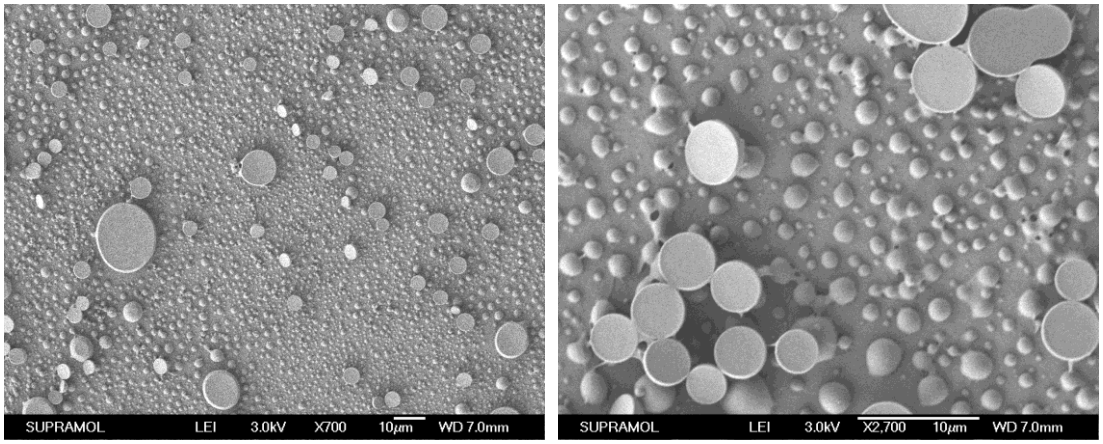

Figure S16. SEM images of SEOP–2 self-assemblies after addition of some amount of methanol.

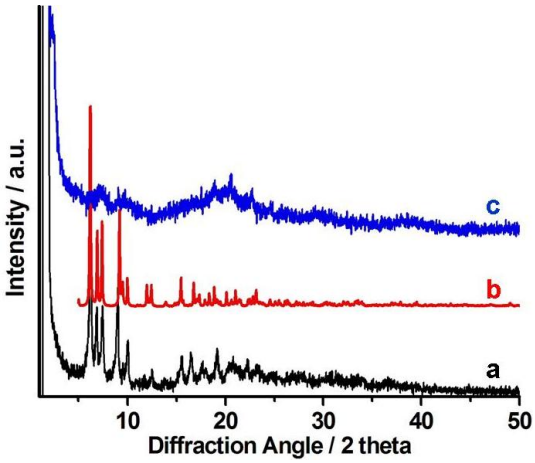

Figure S17. The powder X-ray diffraction patterns and the simulated patterns (a) experimental data for SEOP–1, (b) calculated data for SEOP–1, and (c) experimental data for SEOP–2 in the diffraction angle range of 1-50°.

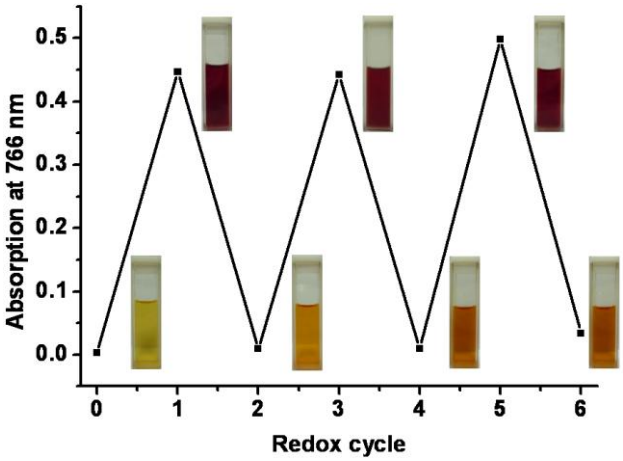

Figure S18. Plot of absorption at 766 nm versus the redox cycle and the corresponding photos.

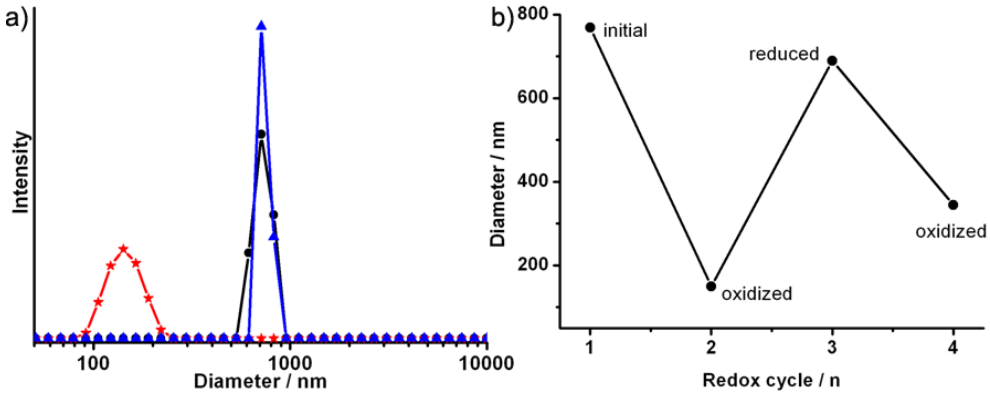

Figure S19. (a) DLS results of SEOP–2 supramolecular self-assemblies during the redox process, and (b) the corresponding diameter change upon oxidization by DDQ and reduction by hydrazine.

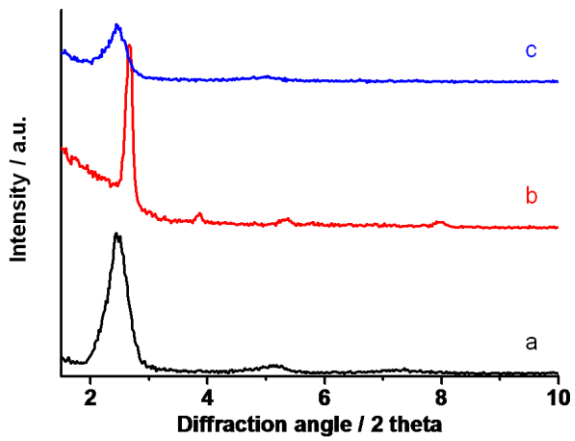

Figure S20. XRD pattern of SEOP–2 self-assemblies during the redox process: a) SEOP–2 self-assemblies in $CHCl_3$:CH_3OH mixture with volume ratio of 4:1, b) after the oxidation of DDQ, and c) after the reduction of hydrazine to b).

Table S1. Full elemental analysis results for SEOP–1 and SEOP–2.

Sample		C (%)	H (%)	N (%)	O (%)	Mn (%)	Mo (%)	Fe (%)
SEOP–1	found	43.51	5.95	2.76	16.54	2.45	23.86	4.88
	calcd	43.97	6.07	2.85	16.92	2.23	23.42	4.54
SEOP–2	found	55.55	8.03	2.34	12.36	1.96	17.45	3.66
	calcd	55.37	8.34	2.07	12.29	1.62	17.01	3.30

Table S2. ESI-MS results for SEOP–1 and SEOP–2, and the corresponding assignment.

Sample	ESI-MS ($gmol^{-1}$)	Assignment
SEOP–1	2216.6	$[M\text{-}2TBA]^-$
SEOP–2	2805.8	$[M\text{-}2DODA\text{-}CHCl_3\text{-}H_2O]^-$